[8] R. A. Rohrer, "The scattering matrix: Normalized to complex n-port load networks," *IEEE Trans. Circuit Theory*, vol. CT-12, pp. 223–230, June 1965.
[9] W. R. Wohlers, "Complex normalization of scattering matrices and the problem of compatible impedances," *IEEE Trans. Circuit Theory*, vol. CT-12, pp. 528–535, Dec. 1965.
[10] M. R. Wohlers, "On scattering matrices normalized to active n-ports at real frequencies," *IEEE Trans. Circuit Theory*, vol. CT-16, pp. 254–256, May 1969.
[11] D. Woods, "General renormalisation transforms for 3-port S-parameters," *Electron. Lett.*, vol. 6, pp. 823–825, Dec. 10, 1970.
[12] D. Woods, "Multiport-network analysis by matrix renormalisation employing voltage-wave S-parameters with complex normalisation," *Proc. Inst. Elec. Eng.*, vol. 124, pp. 198–204, Mar. 1977.
[13] D. Woods, "Reappraisal of computer-corrected network analyser design and calibration," *Proc. Inst. Elec. Eng.*, vol. 124, pp. 205–211, Mar. 1977.
[14] D. M. Kerns and R. W. Beatty, *Basic Theory of Waveguide Junctions and Introductory Microwave Network Analysis*. New York: Pergamon, 1967, p. 108.
[15] D. M. Kerns and R. W. Beatty, *Basic Theory of Waveguide Junctions and Introductory Microwave Network Analysis*. New York: Pergamon, 1967, p. 25.
[16] D. M. Kerns and R. W. Beatty, *Basic Theory of Waveguide Junctions and Introductory Microwave Network Analysis*. New York: Pergamon, 1967, p. 57.
[17] T. Y. Otoshi, "On scattering parameters of a reduced multiport," *IEEE Trans. Microwave Theory Tech.*, vol. MTT-17, pp. 722–724, Sept. 1969.
[18] T. J. Cullen, "An elementary proof of a result used by Otoshi," *IEEE Trans. Microwave Theory Tech.*, vol. MTT-18, p. 171, Mar. 1970.
[19] T. Nemoto and D. F. Wait, "Microwave circuit analysis using the equivalent generator concept," *IEEE Trans. Microwave Theory Tech.*, vol. MTT-16, pp. 866–873, Oct. 1968.
[20] J. K. Hunton, "Analysis of microwave measurement techniques by means of signal flow graphs," *IRE Trans. Microwave Theory Tech.*, vol. MTT-8, pp. 206–212, Mar. 1960.
[21] W. K. Chen, "Relationship between scattering matrix and other matrix representations of linear two-port networks," *Int. J. Electron.*, vol. 38, pp. 433–441, Apr. 1975.
[22] J. G. Evans, "Linear two-port characterization independent of measuring set impedance imperfections," *Proc. IEEE*, vol. 56, pp. 754–755, Apr. 1968.
[23] J. G. Evans, "Measuring frequency characteristics of linear two-port networks automatically," *Bell Syst. Tech. J.*, vol. 48, pp. 1313–1338, May–June 1969.
[24] J. C. Tippet and R. A. Speciale, "A rigorous technique for measuring the scattering matrix of a multiport device with a 2-port network analyzer," *IEEE Trans. Microwave Theory Tech.*, vol. MTT-30, pp. 661–666, May 1982.

Low-Noise, Low Power Dissipation GaAs Monolithic Broad-Band Amplifiers

KAZUHIKO HONJO, TADAHIKO SUGIURA, TSUTOMU TSUJI, AND TOSHIHARU OZAWA

Abstract —**Low-noise, low dc power dissipation GaAs monolithic amplifiers have been developed for use in VHF–UHF mobile radio systems. The developed amplifiers have two-stage construction, where gate width for the first stage is 1000 μm, and for the second stage is 500 μm. Using this circuit configuration, both noise figure and bandwidth have been improved. To maintain the uniformity for the ion-implanted active layers and to reduce gate–source resistance R_S and gate–drain resistance R_D, the "closely spaced electrode FET" was adopted. The FET enables low drain voltage operation, resulting in low dc power dissipation.**

The developed amplifier for the FET threshold voltage $V_T = -0.6$ V provides a 3-dB noise figure, less than 170-mW dc power dissipation, 9-MHz–3.9-GHz bandwidth with 16-dB gain. It can operate under a unipolar power source. When external choke inductors were introduced for the amplifier, 120-mW dc power dissipation has been achieved. It has also been demonstrated that the amplifier for $V_T = -0.6$ V, which is inferior to the amplifier for $V_T = -2.7$ V regarding gain-bandwidth product and power efficiency under the same dc power dissipation, however, has an acceptable performance for use in the mobile radio systems.

Manuscript received September 7, 1982; revised December 22, 1982.
The authors are with Microelectronics Research Laboratories, Nippon Electric Company, Ltd., Kawasaki, Japan.

I. Introduction

Recent advances in GaAs IC technology make it possible to develop multistage GaAs monolithic broad-band amplifiers for general purpose utilization. Expected application fields for the amplifiers are the following:

1) 1-GHz and 2-GHz band mobile radio system;
2) 1.6 = Gbit/s data rate optical communication system;
3) 3-GHz band phased array radar system;
4) intermediate frequency section in microwave communication system;
5) VHF–UHF television.

For these applications, low input and output VSWR, low-noise figure, low dc power dissipation, and high gain are required over a wide frequency range, where there are tradeoff relations among the amplifier characteristics.

Especially in the mobile radio systems, low dc power dissipation (below 150 mW) is a basic requirement for low-noise (less than 3-dB noise figure) broad-band (up to 3 GHz) amplifiers. However, dc power dissipation for the reported amplifiers was as high as 300 mW to 1600 mW [1], [3]–[6]. In addition, the noise figure was not low enough [1], [3], [4], bandwidth was not sufficiently wide [3], [5], [6], and input VSWR was not reduced [5], [9]. Accordingly, to realize GaAs monolithic broad-band amplifiers for use in mobile radio systems, a low dc power dissipation technique has to be developed, considering noise figure, bandwidth, gain, and VSWR. In addition to this, if possible, realizing a unipolar power-source operation for the amplifiers makes them very useful, from a practical point of view.

This paper describes design considerations and performances for newly developed low-noise, low power-dissipation GaAs monolithic broad-band amplifiers for use in VHF–UHF mobile radio systems. It will be shown that, by using the achieved theoretical results which have already been published [1], both noise figure and bandwidth can be improved. The developed amplifiers have two-stage construction, where gate width for the first stage is 1000 μm and that for the second stage is 500 μm. In amplifier fabrication, to improve uniformity for FET active layers and resistive layers, an ion-implantation technique was introduced. The so-called "closely spaced electrode FET" structure, which has been developed for E/D-type GaAs digital IC's [8] in the NEC Research Laboratories, is adopted so that both gate–source resistance R_s and gate–drain resistance R_D can be reduced without recessing the gate. By reducing R_S and R_D, the FET's can operate under low drain voltage with appropriate transconductance g_m, resulting in low dc power dissipation. The nonrecessed FET's maintain uniformity for the ion-implanted layers.

Also, two GaAs monolithic amplifier categories, one for unipolar power-source operation (needs only positive bias supply, $+V_D$), the other for bipolar power-source operation (needs both negative and positive bias supply, $-V_G$ and $+V_D$), are discussed comparatively. It will be demonstrated that the unipolar power-source amplifier, which is inferior to the bipolar power-source

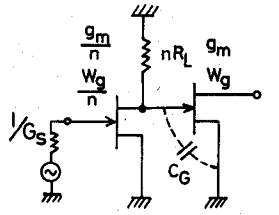

Fig. 1. Equivalent circuit for basic resistor–capacitor coupled amplifier.

amplifier regarding gain bandwidth product and power efficiency, has an acceptable performance for use in mobile radio systems.

II. Circuit Design

Noise figure F, high cutoff frequency f_c, and first-stage voltage gain A_v for a basic resistor capacitor coupled amplifier consisting of source grounded GaAs FET's (Fig. 1) are approximately represented as follows [1]:

$$F \simeq 10\left(\log n + \log \frac{KG_s}{g_m}\right) \tag{1}$$

$$f_c \simeq \frac{1}{2\pi R_L C_G} \cdot \frac{1}{n} \tag{2}$$

$$A_v \simeq -g_m R_L \tag{3}$$

where g_m is the FET transconductance for gate width W_g, n is a scaling number, and K is the constant concerned with device structure. From (1), (2), and (3), it can be understood that a value of n less than unity results in both low-noise figure and broad-band characteristics. Besides, A_v is not changed. A value of n less than unity means that the gate width for the first FET is wider than that for the second stage. Accordingly, in this work, $n = 0.5$ was adopted. To reduce the second term in (1), a comparatively large FET gate width ($W_G = 500$ μm), resulting in large g_m, was introduced. Input VSWR is reduced using an intergate–drain negative feedback because this method doesn't degrade the noise figure seriously [1], [2]. An equivalent circuit for the amplifier is shown in Fig. 2. The interstage circuit consists of a dc block capacitor and a peaking transmission line. As shown in Fig. 2, drain bias voltage can be supplied, either through load resistors ($+V_D$) or through external choke inductors ($+V_D'$). Supplying drain bias voltage through choke inductors avoids dc power dissipation in the load resistors.

Circuit simulation was performed using measured S-parameters for a discrete GaAs FET. As shown in Fig. 3, an 18-dB gain and a 4.1-GHz high cutoff frequency were calculated.

III. Device Design

A. Active Device

To improve uniformity for FET active layers and resistive layers, an ion-implantation technique was introduced. Table I shows an active layer uniformity comparison between ion-implanted layers and epitaxial layers. As shown in the table, regarding FET threshold voltage V_T in a single GaAs wafer, coefficient of sample variation, which is a measure for uniformity for the ion-implanted layers, was one-third of that for the epitaxial layers. In this paper, the "closely spaced electrode FET" was adopted, so that both gate–source resistance R_S and gate–drain resistance R_D could be reduced without recessing the gate. Fig. 4 shows a cross-sectional SEM photograph for the FET. Space values for both gate–source and gate–drain are 0.5 μm, and gate length is 1 μm. Gate metal is Al. AuGe–Ni was used to

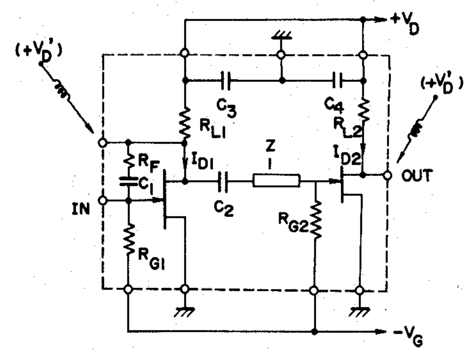

Fig. 2. Equivalent circuit for GaAs monolithic broad-band amplifier.

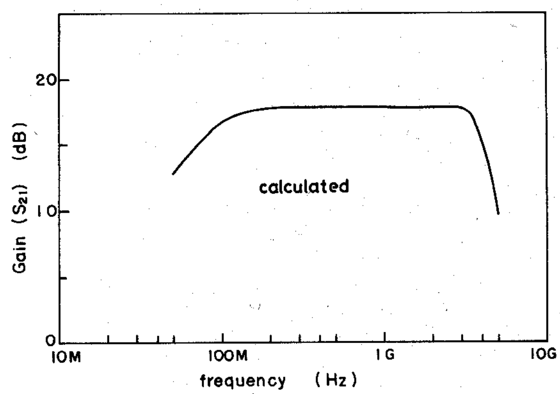

Fig. 3. Simulated gain-frequency characteristic for the GaAs monolithic broad-band amplifier.

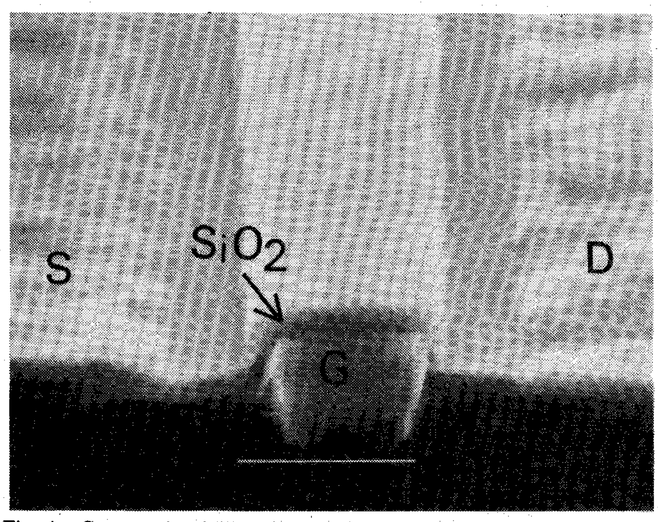

Fig. 4. Cross-sectional SEM photograph for "closely spaced electrode FET".

TABLE I
Uniformity Comparison Between Ion-Implanted Layer and Epitaxial Layer

	$\bar{V}_T$	σ_n	$\sigma_n/\bar{V}_T$
I/I	-1.97V	0.20V	0.10
EPI	-2.24V	0.68V	0.30

$\bar{V}_T$: Average for FET threshold voltage V_T.
σ_n: Standard deviation for V_T.
$\sigma_n/\bar{V}_T$: Coefficient of sample variation for V_T.

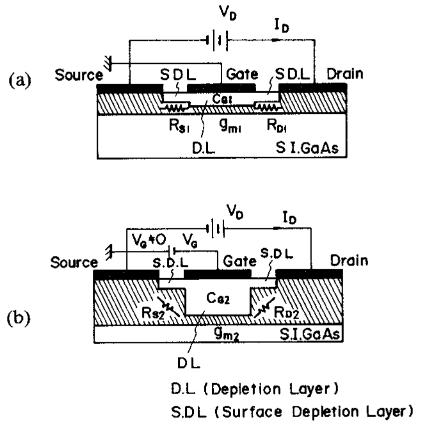

Fig. 5. Qualitative FET operation (a) for unipolar power-source ($V_T = -0.6$ V) and (b) for bipolar power-source ($V_T = -2.7$ V).

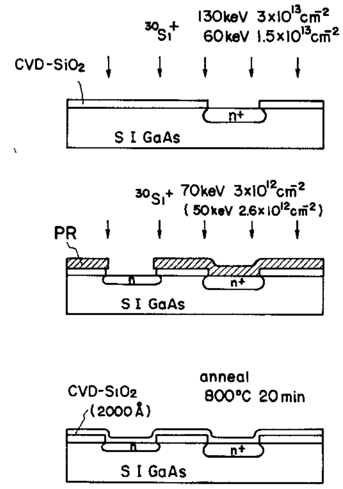

Fig. 6. Ion-implantation process.

form the ohmic contacts. By reducing R_S and R_D, the FET can operate under low drain voltage with proper transconductance g_m. The nonrecessed FET's maintain uniformity for the ion-implanted active layers.

The two categories of GaAs monolithic amplifiers, one for $V_T = -0.6$ V (unipolar power-source operation) and the other for $V_T = -2.7$ V (bipolar power-source operation) were fabricated by controlling the ion-implantation for the FET active layers. In the case of the unipolar power-source operation, the saturation drain current I_{DSS} depends on active layer thickness, since gate bias voltage is 0 V [3]. Therefore, a thin active layer is required to maintain a small I_{DSS} value for low dc power dissipation. However, too thin an active layer causes large values of R_S, resulting in small observed transconductance g_{mo}. Therefore, it was found experimentally, considering I_{DSS} and g_{mo}, that $V_T = -0.6$ V is the best. Drain current I_D for the two categories were chosen so that they are the same. Fig. 5 shows qualitative operation for the two categories. Although transconductance g_m and gate–source capacitance C_G are functions of gate voltage, $g_m/2\pi C_G$, which is a measure of the gain-bandwidth product, is constant in a one-dimensional model [7]. A doping profile for the ion-implanted layers is Gaussian distribution. However, for simplification, assuming doping profiles both for $V_T = -0.6$-V FET (g_{m1}, C_{G1}, R_{S1}) and for $V_T = -2.7$-V FET (g_{m2}, C_{G2}, R_{S2}) as uniform distribution, the following relation can be obtained:

$$\frac{g_{m1}}{2\pi C_{G1}} = \frac{g_{m2}}{2\pi C_{G2}} = \text{const.} \tag{4}$$

Equation (4) implies that intrinsic FET's for the two categories have the same gain bandwidth product. However, since an ion-implanted layer for the $V_T = -0.6$-V FET is thinner than that for the $V_T = -2.7$-V FET, the parasitic resistive element R_{S1} is larger than R_{S2}, as shown in Fig. 5. A well-known relation between observed transconductance g_{mo} and intrinsic transconductance g_{mi}, gate–source resistance R_S is

$$g_{mo} = \frac{g_{mi}}{1 + g_{mi} R_S}. \tag{5}$$

Taking R_S into consideration, a measure of the gain-bandwidth product for the $V_T = -0.6$-V FET (P_{GB1}) and that for the $V_T = -2.7$-V FET (P_{GB2}) are written as follows:

$$P_{GB1} = \frac{g_{m1}}{2\pi C_{G1}(1 + g_{m1} R_{S1})} \tag{6}$$

$$P_{GB2} = \frac{g_{m2}}{2\pi C_{G2}(1 + g_{m2} R_{S2})}. \tag{7}$$

Using (4), (6), and (7), the following relation can be obtained:

$$\frac{P_{GB2}}{P_{GB1}} = \frac{1 + g_{m1} R_{S1}}{1 + g_{m2} R_{S2}}. \tag{8}$$

Since $C_{G1} > C_{G2}$, from (4) and Fig. 5, the following relations are derived:

$$R_{S1} > R_{S2} \quad g_{m1} > g_{m2}. \tag{9}$$

From (8) and (9), the following inequality is derived:

$$\frac{P_{GB2}}{P_{GB1}} > 1. \tag{10}$$

Inequality (10) implies that the gain-bandwidth product for the $V_T = -0.6$-V amplifier is inferior to that for the $V_T = -2.7$-V amplifier. Using electron mobility (3500 $\text{cm}^2/\text{V}\cdot\text{s}$), carrier concentration (2×10^{17} cm^{-3}), surface depletion layer thickness (700 Å), and g_{m2} (75 mS/mm), (8) is roughly calculated as

$$\frac{P_{GB2}}{P_{GB1}} \doteqdot 1.2. \tag{11}$$

For precise discussion, more considerations, including the doping profile, should be taken into account. However, under the first-order approximation, the above-mentioned theory can be used to predict the performance for the $V_T = -0.6$-V amplifier and the $V_T = -2.7$-V amplifier.

The ion-implantation process is shown in Fig. 6. $V_T = -0.6$ V was realized by ${}^{30}S_i^+$ ion implantation to C_r-doped semi-insulating GaAs substrates in selected areas with energy $E = 50$ keV and dose $D = 2.6 \times 10^{12}$ cm^{-2}. An ion-implantation condition for $V_T = -2.7$ V is $E = 70$ keV and $D = 3 \times 10^{12}$ cm^{-2}. Resistive layers were formed by selective double ion-implanted n^+ layers ($E = 130$ keV, $D = 3 \times 10^{13}$ cm^{-2} and $E = 60$ keV, $D = 1.5 \times 10^{13}$ cm^{-2}). The substrates were then coated with CVD-SiO_2 films and annealed at 800°C (20 min) in an H_2 ambient.

Carrier concentration profile and electron mobility profile for the ion-implanted $V_T = -2.7$-V layer, measured using long-gate (250 μm) FET, are shown in Fig. 7. The peak carrier concentration is about 2.5×10^{17} cm^{-3}, and electron mobility at the peak carrier concentration is 3500 $\text{cm}^2/\text{V}\cdot\text{s}$. Typical electron mobility at the carrier concentration for epitaxial layers is about 4000 $\text{cm}^2/\text{V}\cdot\text{s}$. Therefore, it is considered that the ion-implanted layers are approximately equivalent to the epitaxial layers, regarding electron mobility. Fig. 8 shows static characteristics for the $V_T = -2.7$-V FET and the $V_T = -0.6$-V FET. Observed trans-

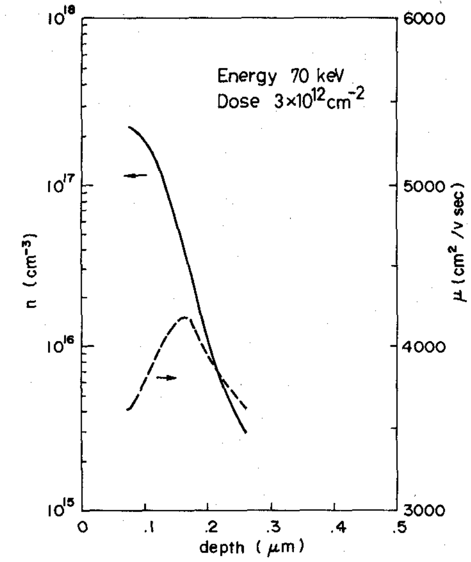

Fig. 7. Carrier concentration profile and electron mobility profile for ion-implanted layer.

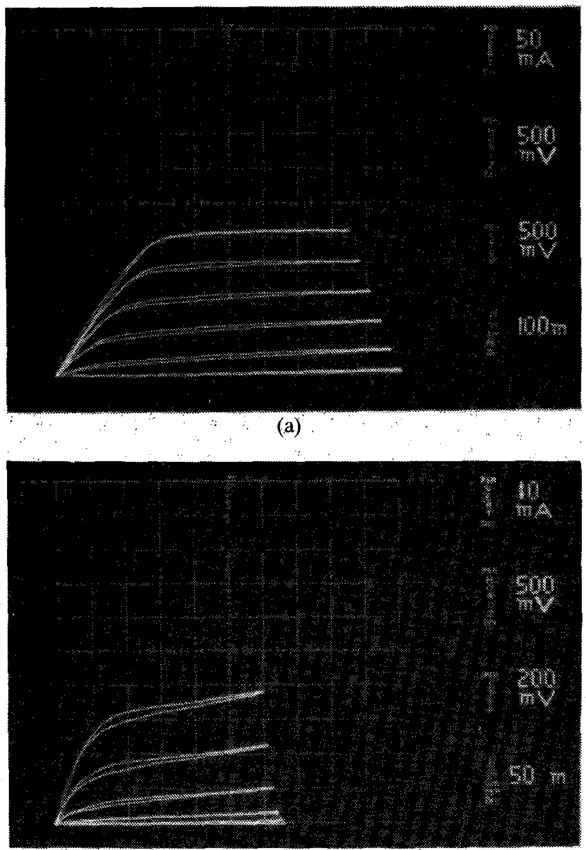

Fig. 8. Static characteristics for (a) $V_T = -2.7$-V FET and (b) $V_T = -0.6$-V FET.

conductance per gate width at saturation drain current g_{mo} is 100 mS/mm for $V_T = -2.7$ V and 75 mS/mm for $V_T = -0.6$ V.

B. Passive Device and Layout

Resistors were made using the same procedure as that for making the active device. Resistors whose values were greater than 1 kΩ were formed by the ion-implanted n layers. Resistors whose values were less than 1 kΩ were formed by the ion-implanted n^+ layers. Average sheet resistivity for the n^+ layers was 134 Ω/□ and standard deviation for the sheet resistivity was 6 Ω/□ in a single GaAs wafer.

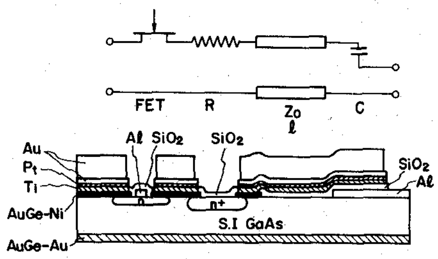

Fig. 9. Cross-sectional view for GaAs monolithic broad-band amplifier.

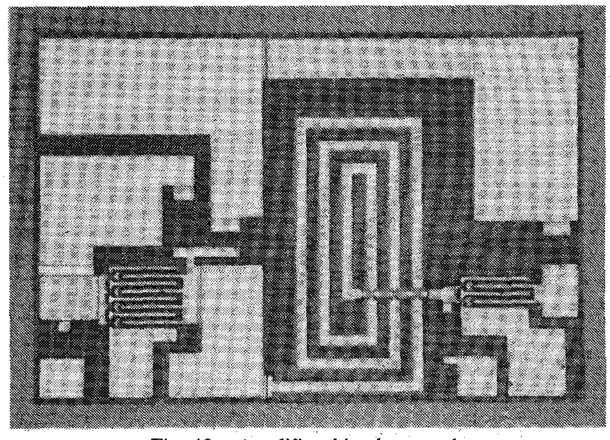

Fig. 10. Amplifier chip photograph.

Capacitors are MIM type. Dielectric material for the capacitors is CVD-SiO_2 ($\epsilon_r \doteqdot 4.8$), which is also used as passivation films for FET's and resistors. The first level metal is Al and the second level metal is T_i–P_t–A_u.

The transmission line used is spiral in shape. Conductor width for the transmission line is 25 μm. A metal system for the conductor is T_i–P_t–A_u. Fig. 9 shows a cross-sectional view for the GaAs monolithic amplifier and its equivalent circuit.

Fig. 10 shows an amplifier chip photograph. Chip size is 1200×800×150 μm.

IV. Results

The GaAs monolithic amplifier chips were mounted in ceramic packages and tested in a 50-Ω system. Figs. 11 and 12 show gain-frequency characteristics and noise figure for the $V_T = -0.6$-V amplifier. The amplifier provides 9-MHz–3.9-GHz bandwidth with 16-dB gain. Less than 3-dB noise figure was achieved in the 90-MHz to 3.5-GHz range. Less than 2.5 input VSWR and less than 3.1 output VSWR were obtained across the frequency range. DC power dissipation was 170 mW. When external choke inductors (30 μmϕ, 2-cm-long Au bonding wires) were used for the drain bias voltage supply, 120-mW dc power dissipation and 4.2-percent power efficiency were achieved.

Meanwhile, the amplifier for $V_T = -2.7$ V provides 9-MHz–4.2-GHz bandwidth with 17-dB gain. When choke inductors were introduced, 100-mW dc power dissipation and 11-percent power efficiency were achieved.

Figs. 13 and 14 show comparison results obtained for the gain-bandwidth product and the input–output power response between the $V_T = -0.6$-V amplifier and the $V_T = -2.7$-V amplifier. As shown in the figures, regarding the gain-bandwidth product and power efficiency, the $V_T = -0.6$-V amplifier is infe-

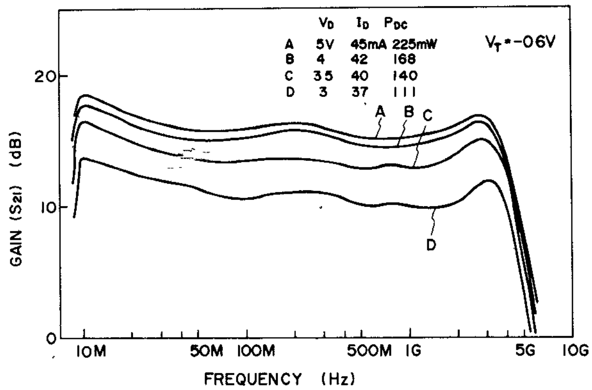

Fig. 11. Gain-frequency characteristics for the $V_T = -0.6$-V amplifier (measured).

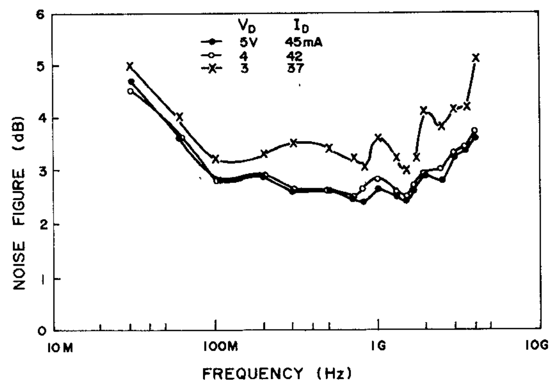

Fig. 12. Noise figure for the $V_T = -0.6$-V amplifier (measured).

TABLE II
PERFORMANCE FOR DEVELOPED GaAs MONOLITHIC BROAD-BAND AMPLIFIER

	bandwidth gain	input VSWR	output VSWR	noise figure	power efficiency
2R-AMP	9MHz–4.2GHz 17dB	45MHz–5GHz <2.5	15MHz–5GHz <1.8	200MHz–3GHz <3.5dB	
1R-AMP	9MHz–3.9GHz 16.7dB	50MHz–3.5GHz <2.5	10MHz–5GHz <3.1	90MHz–3.5GHz <3dB	
2L-AMP	0.3–3.9GHz 17 dB	0.5–3.1GHz <2.5	0.4–3.6GHz <2.5	*	11%
1L-AMP	0.25–3.7GHz 14.7 dB	0.48–3.1GHz <2.5	0.7–4GHz <2.5	*	42%

2R-AMP: Bipolar power-source, through-resistor bias-feed amplifier.
1R-AMP: Unipolar power-source, through-resistor bias-feed amplifier.
2L-AMP: Bipolar power-source, through-choke-inductor bias-feed amplifier.
1L-AMP: Unipolar power-source, through-choke-inductor bias-feed amplifier.
*Not measured, but considered as the same value as the above mentioned data.

rior to the $V_T = -2.7$-V amplifier. However, as shown in Figs. 11 and 12, the $V_T = -0.6$-V amplifier performance is acceptable for use in the mobile radio systems. Developing the $V_T = -0.6$-V amplifier, the unipolar power-source operation under low dc power dissipation could be realized. From a practical point of view, the unipolar power-source operation is very useful for the system. The performance for the amplifiers is summarized in Table II.

V. CONCLUSIONS

Low-noise, low dc power dissipation GaAs monolithic amplifiers have been developed for VHF–UHF mobile radio systems. The developed amplifiers have two-stage construction, where gate

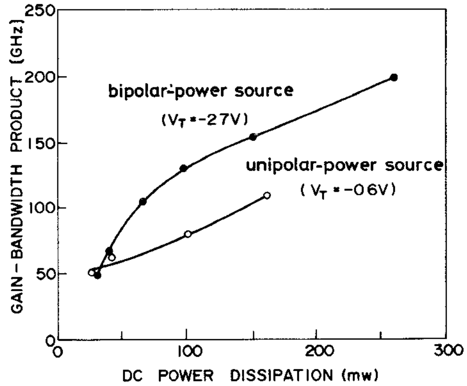

Fig. 13. Gain-bandwidth product comparison between the $V_T = -0.6$-V amplifier and the $V_T = -2.7$-V amplifier (measured using choke inductors).

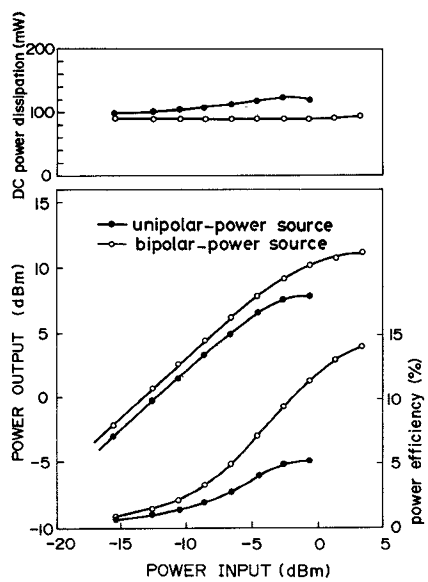

Fig. 14. Input-output power response comparison between the $V_T = -0.6$-V amplifier and the $V_T = -2.6$-V amplifier (measured using choke inductors).

width for the first stage is 1000 μm and for the second stage is 500 μm. Using this circuit configuration, both noise figure and bandwidth could be improved. To maintain the uniformity for the ion-implanted active layers and to reduce R_S and R_D, the "closely spaced electrode FET" was adopted. The FET enabled low drain voltage operation, with low dc power dissipation.

The developed amplifier for $V_T = -0.6$ V, which can operate under a unipolar power-source, provides a 3-dB noise figure, less than 170-mW dc power dissipation, 9-MHz–3.9-GHz bandwidth with 16-dB gain. When external choke inductors were introduced for the amplifier, 120-mW dc power dissipation has been achieved. It has also been demonstrated that the amplifier for $V_T = -0.6$ V, which is inferior to the amplifier for $V_T = -2.7$ V regarding the gain-bandwidth product and power efficiency, has an acceptable performance for the mobile radio systems.

ACKNOWLEDGMENT

The authors would like to thank M. Ohyagi for technical assistance and H. Itoh for taking the SEM photograph. They would also like to thank Y. Takayama, M. Muta, and H. Katoh for their constant encouragement throughout this work.

REFERENCES

[1] K. Honjo, T. Sugiura, and H. Itoh, "Ultrabroad-band GaAs monolithic amplifier," *IEEE Trans. Microwave Theory Tech.*, vol. MTT-30, pp. 1027–1033, July 1982; also in *Electron. Lett.*, vol. 17, no. 24, pp. 927–928, Nov. 1981.

[2] K. Honjo and Y. Takayama, "GaAs FET ultrabroad-band amplifiers for Gbit/s data rate systems," *IEEE Trans. Microwave Theory Tech.*, vol. MTT-29, pp. 629–636, July 1981.
[3] H. P. Weidlich, J. A. Archer, E. Pettenpaul, F. A. Petz, and J. Huber, "A GaAs monolithic broadband amplifier," in *1981 IEEE Int. Solid-State Circuit Conf. Dig.*, Feb. 1981, pp. 192–193.
[4] D. B. Estreich, "A wideband monolithic GaAs IC amplifier," in *1982 IEEE Int. Solid-State Circuit Conf. Dig.*, Feb. 1982, pp. 194–195.
[5] S. Hori, K. Kamei, M. Takematsu, T. Chigira, H. Ishimura, and S. Okano, "Direct-coupled GaAs monolithic IC amplifiers," in *IEEE 1982 Microwave and Millimeter-wave Monolithic Circuit Symp. Dig.*, June 1982, pp. 16–19.
[6] M. Nishiuma, S. Nambu, M. Hagio, and G. Kano, "A GaAs monolithic low-noise wideband amplifier," in *Proc. 9th Int. Symp. GaAs and Related Compounds*, Sept. 1981, pp. 425–430.
[7] R. E. Williams and D. W. Shaw, "Graded channel FET's: Improved linearity and noise figure," *IEEE Trans. Electron Devices*, vol. ED-25, pp. 600–605, June 1978.
[8] T. Furutsuka, T. Tsuji, F. Katano, A. Higashisaka, and K. Kurumada, "Ion-implanted E/D type GaAs IC technology," *Electron. Lett.*, vol. 17, no. 25/26, pp. 944–945, Dec. 1981.
[9] D. P. Hornbuckle and R. L. Van Tuyl, "Monolithic GaAs direct-coupled amplifiers," *IEEE Trans. Electron Devices*, vol. ED-28, pp. 175–182, Feb. 1981.

Permittivity Measurements of Lossy Liquids at Millimeter-Wave Frequencies

LUIGI ZANFORLIN

***Abstract*—A measurement system is described which allows the determination of the complex permittivity of high-loss liquids at millimeter waves. Basically, the setup consists of a waveguide interferometer whose unknown arm embodies a liquid holder irradiated by an open-ended rectangular waveguide. The sample thickness is varied by means of a piston driven by a micrometer screw. The bridge output then is read as a function of the liquid thickness. Best fitting between experimental and computed data through a suitable model of the system enables the permittivity to be determined. The system can operate, with high sensitivity, over the whole frequency range of the dominant mode propagating in the waveguide setup employed. System performance is described through a set of experimental results obtained on ethanol, methanol, and pure water at 20° C and 70 GHz.**

I. Introduction

Measurements of the complex dielectric constant of liquids in the largest possible frequency range have received qualified attention from experimenters of different fields. Thus, Hollecker, Goulon *et al.* performed measurements of 2 and 5 MHz [1], and Goulon, Roussy *et al.* performed measurements of solutions in the far IR [2]. Szwarnowski and Sheppard worked at 70 GHz by using holders designed for this frequency [3].

In this paper, a wide-band measurement system in the millimeter-wave range is presented, following a previous method to measure the permittivity of a living cell's sediment obtained from a suspension into a watery medium [4], [5]. The very high sensitivity experienced with this technique in the range 65–85 GHz, in spite of the large attenuation constant of water, has suggested extending the basic method to lossy liquid permittivity measurements.

For this purpose, a proper sample holder to be kept in contact with the flange of an open-ended waveguide has been studied. Thus, the high-frequency difficulties associated with the use of cavity resonators or waveguides as sample holders have been avoided, and a broad-band precise measurement system has been obtained. The system performance has been evaluated by carrying out measurements on ethanol, methanol, and pure water at 20° C and 70 GHz.

Manuscript received May 6, 1982. This work was supported by the Italian National Research Council (CNR).
The author is with the Istituto di Elettrotecnica ed Elettronica, Universita di Palermo, Viale delle Scienze, Palermo, Italy 90128.

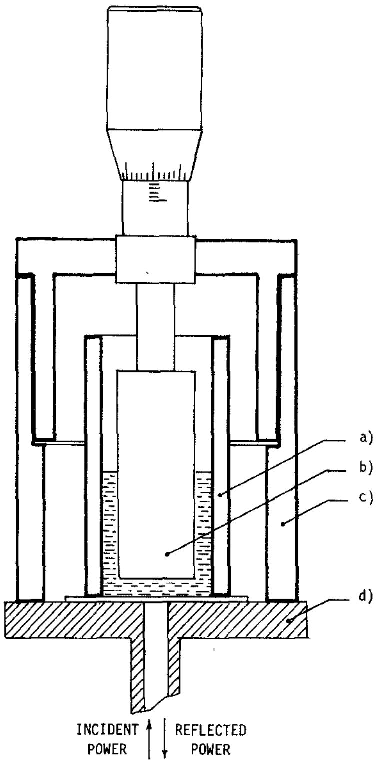

Fig. 1. Cell for lossy liquids permittivity measurements. a) Glass sample holder. b) Teflon piston. c) Micrometer screw socket. d) Waveguide flange.

II. Measuring System

The liquid dielectric to be tested is put in the glass sample holder shown in Fig. 1. The bottom of the sample holder consists of a slide 0.15 mm thick, and its underside is irradiated by a contacting open-ended flanged rectangular waveguide. The signal reflected from the holder is varied by changing the sample thickness by means of a piston driven by a micrometer screw; the piston position can be set to within 5 μm.

Both the socket of the micrometer and the bottom of the sample holder are trued with the waveguide and are cemented to the waveguide flange. Thus, unwanted movements while turning the micrometer are avoided, and a correct and repeatable placement of the sample is ensured. In the experiments, a teflon piston is used in order to avoid chemical reactions with the liquid sample.

Results can be shown to be independent of the piston material, provided that its electrical characteristics are different enough from those of the sample.

The signal reflected from the sample holder is compared with a constant reference signal by means of the null interferometric

0018-9480/83/0500-0417$01.00 ©1983 IEEE